



RESEARCH ACTIVITIES

Materials Molecular Science

Extensive developments of new functional molecules and their assemblies are being conducted in three Divisions of Electronic Structures, Electronic Properties, and Molecular Functions, and one division for visiting professors, in an attempt to discover new phenomena and useful functions. The physical (electric, optical, thermal and magnetic) properties on new functional materials, the chemical properties like enzymes, catalysis and photochemistry, the exploitation of new spectroscopic methods for materials molecular science, and technological applications like solar cells and transistors are investigated in this department.

Exploitations of Novel Spectroscopic Methods Using Synchrotron Radiations and Lasers for Materials Science

Department of Materials Molecular Science
Division of Electronic Structure



YOKOYAMA, Toshihiko
Professor

NAKAGAWA, Takeshi
WANG, Heng
EGUCHI, Keitaro
NAKANO, Hirohito
UOZUMI, Madoka



TAKAGI, Yasumasa
Assistant Professor

Assistant Professor*
Post-Doctoral Fellow
Graduate Student
Graduate Student
Technical Fellow



UEMURA, Yohei
Assistant Professor

USUI, Chika
FUNAKI, Yumiko
TOYAMA, Yu
FUKUTOMI, Yukiyo
YASUI, Yuco
WATANABE, Yoko

KANEKO, Yasushi
INOUE, Mika

Technical Fellow
Secretary
Secretary
Secretary
Secretary
Secretary

Nano. Platform Manager
Nano. Platform Manager

To develop novel functional materials, it is also essentially important to exploit new characterization methods that improve spatial and time resolving powers substantially and allow one to investigate the materials in operand conditions. In our group, we are interested in the developments of new spectroscopic methods for materials science using synchrotron radiation and lasers. Especially, we have been investigated surface and thin-film magnetism and related magnetic materials for the last decade. Recently, to investigate surface reaction process in working condition, we began to exploit hard x-ray photoelectron spectroscopy at ambient pressure.

1. Novel Magnetic Nanoscope: Ultraviolet Magnetic Circular Dichroism Photoelectron Emission Microscope (UVMCD PEEM)¹⁾

Since we discovered dramatic enhancement of visible and ultraviolet photoemission magnetic circular dichroism of 3d transition metal ultrathin films in the vicinity of the work function threshold,¹⁾ we have been exploiting UVMCD PEEM to visualize magnetic domains with a spatial resolution of ~30 nm and a time resolution of ~100 fs. Compared to X-ray MCD PEEM that has now become a widely established technique, this technique is advantageous in that the measurements can be performed in laboratory and the time resolution of ~100 fs can easily be achieved by using ultrashort pulsed lasers that are commercially available.

The light source is a wavelength-tunable high-power mode-locked Ti:Sapphire laser, and by using the second-, third- and fourth-order harmonics available photon energies are 3.0–6.0 eV with sufficient intensity. Two-photon processes are also available for the requirement of higher photon energies.

The pulse width is ~200 fs and the ultrafast pump-and-probe experiment can be performed. Figure 1 is the demonstrative magnetic domain images of ~15 monolayer Ni films grown epitaxially on Cu(001) during hydrogen adsorption with almost real-time observation interval. Bright and dark contrasts stand for upward and downward magnetic domains. As H₂ adsorbs on the Ni surface, it is clearly found that the shape of the magnetic domains becomes simpler so that the length of domain wall may be reduced. This originates from stabilization of the perpendicular magnetic anisotropy of the Ni films upon hydrogen adsorption. To reduce instability at the domain walls with a large perpendicular magnetic anisotropy, the domain wall length is shorter with H₂ adsorption.

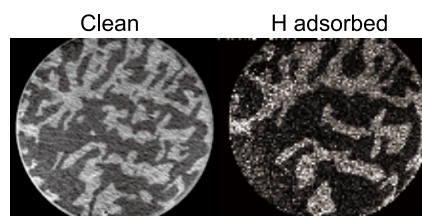


Figure 1. Magnetic domain images of ~15 ML Ni on Cu(001) at 300 K before and after hydrogen adsorption. The field of view is 100 μ m.

2. Ambient Pressure Hard X-Ray Photo-Electron Spectroscopy

In order to investigate Pt-based catalysts in polymer electrolyte fuel cells under working conditions, we are exploiting hard x-ray photoelectron spectroscopy in an ambient pressure. Ambient pressure soft x-ray photoelectron spectroscopy is now available in several third-generation synchrotron facilities

in the world and allows one to characterize the surface of the specimen at ~ 100 Pa. However, the maximum pressure is still too small to study wet materials. Because of substantially longer mean free paths of electrons with much higher electron kinetic energies, the usage of hard x-rays can extend the pressure range up to ~ 3000 Pa that corresponds to the vapor pressure of water at room temperature. Up to now, no reports concerning this technique are seen in the literatures.

We have joined NEDO (New Energy and Industrial Technology Development Organization) fuel cell project and installed an ambient pressure hard x-ray photoelectron spectrometer in Beamline 36XU of SPring-8, as shown in Figures 2(a) and 2(b). The hard x-rays from the undulator source with photon energies of 6–8 keV, are monochromatized by four Si crystals, and the total energy resolution including the electron energy analyzer is ~ 0.35 eV for practical use. Figure 2(c) shows the Au 4f spectra of Au foil by varying the environmental pressure. Up to 3000 Pa N_2 , we have successfully obtained good Au 4f spectra of Au foil without any discharging problem concerning high voltages applied to the electron lenses. We have tried to measure Pt 3d spectra [Figure 2(d)] of the Pt-C electrode in sulfuric acid solution with Nafion membrane by applying the voltage to conduct water electrolysis. With increasing the applied voltage, Pt is gradually oxidized to provide larger Pt–OH and Pt–O signals. At 1.8 V, the electrolysis of water takes place and again the Pt–O signal is reduced. Since the performance of the spectrometer is found to be excellent, an application to real fuel cell systems is desired as soon as possible.

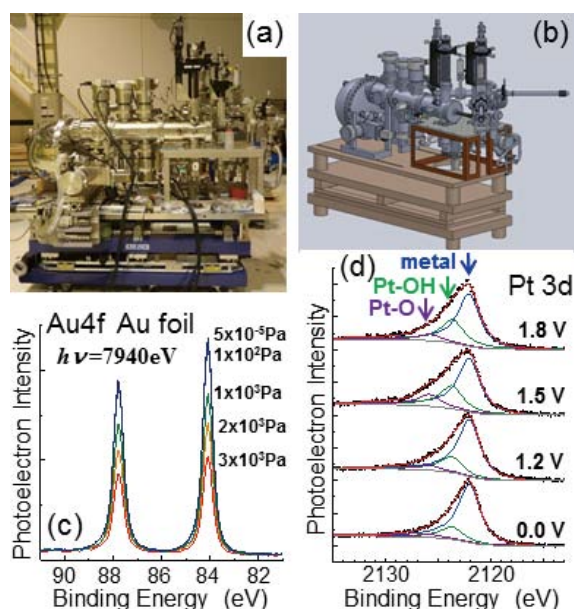


Figure 2. Photo (a) and schematic drawing (b) of the ambient pressure hard x-ray electron spectrometer. (c) Au 4f photoelectron spectra of Au foil under N_2 . (d) Pt 3d photoelectron spectra of the Pt-C/Nafion/ $H_2SO_4(aq)$ /Pt system under 2000 Pa O_2 atmosphere by varying the voltage applied to the Pt-C electrode.

3. Anisotropic Thermal Expansion and Invar/Anti-Invar Effects in $MnNi^3$

An Invar alloy $Fe_{66}Ni_{34}$ that shows anomalously small thermal expansion over a wide temperature range was discovered in 1897. Basically, the coexistence of the different electronic states in Fe compensates for thermal expansion. The detailed origin of the Invar effect is however a famous long-standing problem. Previously we have studied local thermal expansion and its quantum effect.²⁾ In this work, anisotropic thermal expansion in fct $Mn_{88}Ni_{12}$ alloy, which has a martensitic shape memory effect, was investigated by EXAFS and the path-integral simulations.³⁾

In the lattice constants, the a axis shows somewhat larger thermal expansion than usual, while the c axis exhibits almost no thermal expansion. The environment around Mn is found to be really tetragonally distorted, while the Ni environment is regarded as cubic. It should be noted here that in spite of the fact that the average x-ray structure is fct, the local structures of Mn and Ni are essentially different. It is also clearly found that the theoretical simulations based on the low-spin/high-spin two-state model successfully reproduce all the experimental lattice constants and bond distances. This confirms that the two inequivalent bonds around Mn are regarded as the bonds within the bc/ca and ab planes. Consequently, the present anisotropic thermal expansion is explained by the cooperative Invar/anti-Invar effects in the Mn atom, where the tetragonally distorted more stable low-spin Mn state gives a smaller atomic radius within the ab plane and a larger radius along the c axis than the spherical one of the HS state, as depicted in Figure 3(c).

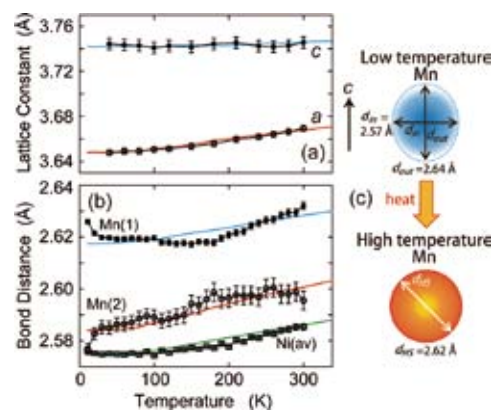


Figure 3. Experimental and simulated (a) lattice constants and (b) bond distances. (c) Schematic model of electronic structure change in Mn at low and high temperatures.

References

- 1) T. Nakagawa and T. Yokoyama, *J. Electron Spectrosc. Relat. Phenom.* **185**, 356 (2012).
- 2) T. Yokoyama and K. Eguchi, *Phys. Rev. Lett.* **107**, 065901 (2011).
- 3) T. Yokoyama and K. Eguchi, *Phys. Rev. Lett.* **110**, 075901 (2013).

* Present Address; Department of Molecular and Material Sciences, Interdisciplinary Graduate School of Engineering Sciences, Kyushu University, Kasuga Koen 6-1, Kasuga, Fukuoka 816-8580, Japan

Design and In-Situ Characterization of Catalyst Surfaces

Department of Materials Molecular Science
Division of Electronic Structure



TADA, Mizuki
Associate Professor (–March, 2013)*

MAITY, Niladri
ZHANG, Shenghong
SAIDA, Takahiro
WAKI, Minoru

Post-Doctoral Fellow
Post-Doctoral Fellow
Post-Doctoral Fellow
Post-Doctoral Fellow



MURATSUGU, Satoshi
Assistant Professor†

SODE, Aya
KITYAKARN, Sutasinee
TRAN, Quang Thuong
WANG, Fei
ISHIGURO, Nozomu
USUI, Chika
GONDO, Makiko
FUKUTOMI, Yukiyo

Post-Doctoral Fellow
Post-Doctoral Fellow
JENESYS Program Visiting Scientist
Graduate Student
Graduate Student[‡]
Technical Fellow
Technical Fellow
Secretary

We have focused on the preparation of new catalyst surfaces by using metal complexes, metal nanoparticles, and metal oxides and in situ characterization of solid catalysts under catalyst working conditions.

1. Preparation and Discontinuous Property of Methane Steam Reforming of Ni/Ordered $\text{Ce}_2\text{Zr}_2\text{O}_x$ Catalysts¹⁾

Methane steam reforming is one of the key reactions to produce hydrogen. We prepared Ni catalysts on an ordered $\text{Ce}_2\text{Zr}_2\text{O}_x$ solid-solution support ($x = 7-8$) with a regular arrangement of Ce and Zr ions for CH_4 steam reforming to produce H_2 and CO . The catalytic performance of the Ni/ $\text{Ce}_2\text{Zr}_2\text{O}_x$ catalysts strongly depended on the oxygen content of $\text{Ce}_2\text{Zr}_2\text{O}_x$, and we found a unique discontinuity in the CH_4 steam-reforming activity at $x = 7.5$ (Figure 1).

Ni/ $\text{Ce}_2\text{Zr}_2\text{O}_7$ catalyst was stable, resulting in a remarkably catalytic performance. The discontinuity in the catalytic performance at $x = 7.5$ may be related to the oxygen storage capacity of $\text{Ce}_2\text{Zr}_2\text{O}_x$. The reduction of NiO_y strongly depended

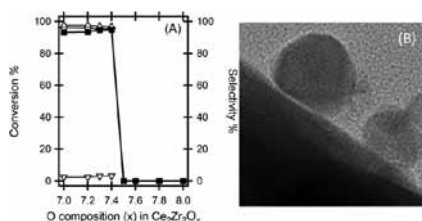


Figure 1. (A) CH_4 steam-reforming performance of Ni/ $\text{Ce}_2\text{Zr}_2\text{O}_x$ at 973 K. The oxygen content x was changed by the reaction with O_2 and Ni/ $\text{Ce}_2\text{Zr}_2\text{O}_7$ at 773 K ■ (with bold line): CH_4 conv.%, \triangle : CO selectivity %, ∇ : CO_2 selectivity %, and \diamond : H_2 selectivity %. (B) A TEM image of the Ni catalyst.

on the nature of the $\text{Ce}_2\text{Zr}_2\text{O}_x$ support. In the range of $7 \leq x < 7.5$, Ni and $\text{Ce}_2\text{Zr}_2\text{O}_x$ were reduced to the metallic state and the $\text{Ce}_2\text{Zr}_2\text{O}_7$ phase, respectively, under the reaction conditions; the reduction was due to CH_4 . In the range of $7.5 \leq x \leq 8$, however, NiO_y was converted to NiO and $\text{Ce}_2\text{Zr}_2\text{O}_x$ remained unchanged under the reaction conditions. The oxidation of Ni nanoparticles on $\text{Ce}_2\text{Zr}_2\text{O}_x$ ($7.5 \leq x \leq 8$) was due to H_2O .

The oxygen storage and release processes rapidly occur at $x < 7.5$ compared with $x \geq 7.5$. In the range of $7 \leq x < 7.5$, lattice oxygen atoms in $\text{Ce}_2\text{Zr}_2\text{O}_x$ readily migrate from the bulk to the surface, at which they react with CH_4 to form the resultant $\text{Ce}_2\text{Zr}_2\text{O}_7$ phase. The transport of oxygen atoms at the interface between NiO_y nanoparticles and a $\text{Ce}_2\text{Zr}_2\text{O}_x$ support and/or the spillover of oxygen atoms at the boundary may be key issues in the chemical event.

2. Imaging of Pt/C Cathode Catalyst Layers in MEA for PEFC by X-Ray Laminography XAFS²⁾

Polymer electrolyte fuel cells (PEFCs) are among the most efficient clean energy technologies, but practical application in automobiles remains challenging because of the high cost and insufficient durability of cathode catalysts. The deactivation and unfavorable dissolution of Pt catalysts at cathode under PEFC operating conditions are serious to be tackled. However, direct observation of the chemical states of Pt catalysts in a membrane electrode assembly (MEA) for PEFC is not achieved in a non-destructive manner.

X-ray Computed Laminography (XCL) is applicable to partial three-dimensional imaging of such a shaped sample. In XCL, the rotation axis of a sample is not fixed at 90° with respect to incident X-ray beam, and the sample is inclined. We succeeded in measuring XCL-XAFS combining XCL imaging

technique and XAFS spectroscopy by changing the energies of incident X-rays for XCL. The reconstruction images of XCL-XAFS revealed not only the morphology of cathode catalyst layer but also the distribution of Pt catalysts inside the catalyst layer.

The spatio-distribution of the Pt catalysts was visualized by mapping Pt L_{III} -edge intensity, which corresponds to a difference in the intensity of X-ray absorption at 11.572 keV (isosbestic point of Pt and PtO₂) from that at 11.496 keV (before Pt L_{III} -edge). We reconstructed 3D images of the distributions of Pt nanoparticles in the cathode catalyst layer in the fresh and degraded MEAs. The distribution of the Pt catalyst remarkably changed after the degradation process of MEA, and several aggregation spots of the Pt catalyst and large cavities in the cathode catalyst layer were observed (Figure 2 (A)). The Pt distribution was heterogeneous throughout the entire cathode catalyst layer, which suggests that Pt migration, aggregation, and cracking spread throughout the cathode catalyst layer in the degraded MEA.

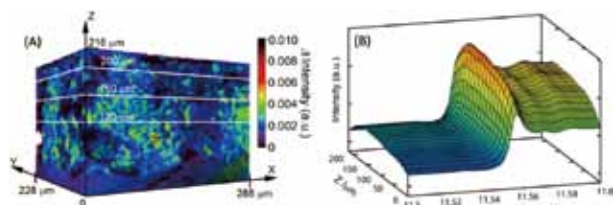


Figure 2. (A) The distribution of the Pt catalyst inside the cathode catalyst layer of the degraded MEA by XCL-XAFS. (B) Depth-resolved XCL-XANES spectra for the degraded MEA.

Depth-resolved XANES spectra were successfully obtained by integrating 3D-Laminography-XANES spectra over the X–Y plane at each depth in the X-ray energy range of 11.439–11.608 keV (Figure 2 (B)). Difference in the edge intensity of the Pt L_{III} -edge XANES spectra indicates difference in the Pt quantity in the MEAs along the Z depth. A series of depth-resolved Laminography-XANES spectra of the degraded MEA were wavy to the Z depth, probably reflecting the degradation of the MEA.

The newly developed XCL-XAFS technique provided the three-dimensional images of Pt quantity in the fresh and degraded MEAs enabled the visualization of aggregation behavior induced under PEFC operating processes. The 3D-Laminography-XAFS method would be promising for visualizing heterogeneous structural information in MEAs in order to address critical issues on the performance and property of practical PEFCs.

Award

KITYAKARN, Sutasinee; Poster Prize Award (ISHHC-16).

* Present Position; Professor, Research Center for Materials Science, Nagoya University

† Present Address; Graduate School of Science, Nagoya University

‡ carrying out graduate research on Cooperative Education Program of IMS with The University of Tokyo

3. Ethynylpyridine-Functionalized Pt/Al₂O₃ Catalyst with Induced Chirality for Hexose Sugar Oxidation³⁾

Uronic acids are monosaccharide derivatives in which primary hydroxyl group at the terminal carbon is oxidized to a carboxylic acid. To prepare glucuronic acid, the hydroxyl group at the 6-position of glucose must be selectively oxidized without over-oxidizing the secondary alcohols at other positions. We prepared a heterogeneous Pt nanoparticle catalyst with a sugar-binding ethynylpyridine (EPy) site (EPy/Pt/Al₂O₃) for the selective oxidation of hexose sugars to their corresponding uronic acids. Compared with a non-EPy-functionalized Pt/Al₂O₃ catalyst, EPy/Pt/Al₂O₃ enhanced reaction rates for the selective oxidation of the 6-OH groups of hexose sugars.

Titration with octyl β-D-glucopyranoside monitored by UV/vis and CD spectroscopy revealed that EPy acted as a binding site for hexose sugar, resulting in a complex of the EPy moiety and the hexose sugar with induced chirality. When Oct-β-D-Glc was added, an induced CD (ICD) signal with negative Cotton effect was observed in the region of the EPy ligand absorption (Figure 3 (A)). An ICD signal with positive Cotton effect was also observed after the addition of the enantiomer, octyl β-L-glucopyranoside. The ICD signals of the EPy ligand on the EPy/Pt/Al₂O₃ catalyst surface depended on the chirality of the hexose sugars, which demonstrated that binding interaction between the EPy ligand and the hexose sugars existed on the catalyst surface (Figure 3 (B)). The positive binding of the hexose sugars to EPy through intermolecular host–guest interaction would be enhanced the reaction rates of the selective oxidation on the Pt nanoparticle catalyst.

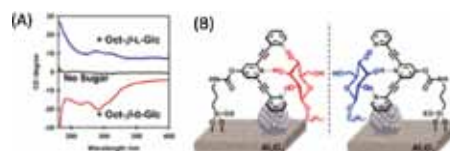


Figure 3. (A) CD spectra of the mixture of Pt/Al₂O₃ and octyl β-glucopyranoside in CH₂Cl₂. (B) The suggested host–guest interaction of EPy and the hexose sugar.

References

- 1) M. Tada, S. Zhang, S. Malwadkar, N. Ishiguro, J. Soga, Y. Nagai, K. Tezuka, H. Imoto, S. O. –Y. –Matsuo, S. Ohkoshi and Y. Iwasawa, *Angew. Chem., Int. Ed.* **51**, 9361–9365 (2012) (Hot Paper).
- 2) T. Saida, O. Sekizawa, N. Ishiguro, K. Uesugi, M. Hoshina, T. Uruga, S. Ohkoshi, T. Yokoyama and M. Tada, *Angew. Chem., Int. Ed.* **51**, 10311–10314 (2012).
- 3) M. Waki, S. Muratsugu and M. Tada, *Chem. Commun.* **49**, 7283–7285 (2013) (Inside Back Cover).

Magnetic Resonance Studies for Functional Molecular-Based Solids

Department of Materials Molecular Science
Division of Electronic Properties



NAKAMURA, Toshikazu
Associate Professor



FURUKAWA, Ko
Assistant Professor*

TAKAHASHI, Seiya
ABE, Hitomi

Graduate Student†
Secretary

Magnetic resonance measurements are advantageous for studying fundamental electronic properties and for understanding the detailed electronic structures of molecular based compounds. Developing an understanding of the electronic phases and functionality of these materials enables us to perform systematic investigations of low-dimensional, highly-correlated electron systems and functional materials. Competition between the electronic phases in molecular-based conductors has attracted much attention. The investigations of such electronic phases by magnetic resonance measurements are important to understanding unsolved fundamental problems in the field of solid state physics, and to explore novel functionalities in the field of material science.

In this study, we performed broad-line NMR and ESR measurements on molecular-based conductors to understand electron spin dynamics and functionality in low-temperature electronic phases.

1. Time-Resolved ESR Spectroscopy Investigation of Photoconduction Mechanism in Covalent Organic Framework (COF) Materials

Covalent organic framework (COF) materials are porous crystalline materials. They attracted much attention because of their functionalities. Recently, a variety of COF materials based on the Donor-Acceptor (D-A) system have been developed. Jiang and coworkers synthesized a variety of D-A type COFs such as NDI-ZnPc, PyDI-ZnPc and ZnPc-NDI-HHTP. While molecules are connected by tight covalent bonds within the two-dimensional layers, the molecules stack to form one-

dimensional columns perpendicular to the planes. They show pronounced photo-conducting behavior. The possible photo-conduction origin is the electron transfer between donor and acceptor. However, the detail mechanism is an open question. We performed time-resolved photo-excited ESR spectroscopy for a series of D-A type COF materials to investigate the photo-conduction mechanism. After photo-excitation to D-A type COFs, an ESR signal originated from the charge-separated state was observed, which could not be observed in isolated molecules. As for ZnPc-NDI-COF, we can observe the charge-separated ESR signal even at R.T., indicating long lifetime of the photo-excited carriers. Actually, the lifetime of the photo-excited charge-separated states in ZnPc-NDI-COF are estimated as 865 μ s at 80 K and 1.8 μ s at 280 K.

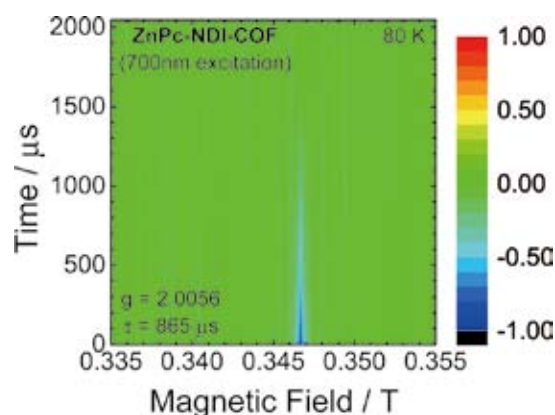


Figure 1. 2D pulsed TR-ESR spectra for ZnPc-NDI-COF. The normal axis represents the ESR signal intensity. The color scale denotes the signal intensity. Positive and negative values indicate the absorption and emission of microwaves, respectively.

2. Simultaneous Control of Carriers and Localized Spins with Light in Organic Materials

Photoconduction and its related phenomena have been known for quite some time, and have attracted a significant amount of scientific attention. Photoconduction is applied in devices, sensors, detectors, and energy converters, such as charge-coupled devices, complementary metal oxide-semiconductor image sensors, and photovoltaic cells, in addition to other advanced applications under investigation. In all known photoconductors, photoexcitation (PE) controls only the carriers. Herein, a new photoconductor is reported, in which the carriers and localized spins can be simultaneously controlled with UV irradiation. This material transforms from a semiconductor to a metal under irradiation, distinguishing it from all existing photoconductors. Furthermore, an interaction between the carriers and localized spins has been discovered, which enables the localized spins to be controlled and detected by the carriers and vice versa. In addition, the photoconduction is unique because it exhibits wavelength selectivity. The selectivity means that the photoconduction mechanism is different from currently known mechanism. No material has been found in which the carriers and localized spins can be simultaneously generated with light. If the carriers and localized spins are controlled using light (i.e., via PE), it may be possible to enhance this control over a wider range, beyond the restrictions of thermodynamic equilibrium. In order to find such a material, a promising starting point is to investigate charge-transfer salts consisting of a photochemical redox pair, because, under irradiation, the redox reaction transfers a larger number of electrons between pairs, and thus produces, by far, a larger number of carriers and localized spins than using PE alone. Following a series of examinations of a variety of charge-transfer salts, focus was placed on salts of $[\text{Ni}(\text{dmit})_2]_n^-$ (dmit = 1,3-dithiol-2-thione-4,5-dithiolate; $0 \leq n \leq 2$) and methyl viologen (MV_n^+). $\text{Ni}(\text{dmit})_2$ molecules are known to form conducting solids with multiredox properties, while the MV is expected to be a spin source under irradiation because of its characteristic photochemical redox reactivity. Herein, a strategy for realizing photomagnetic conductors is proposed and demonstrated based on the electrical and magnetic properties of $\text{MV}[\text{Ni}(\text{dmit})_2]_2$.

3. Organometallic Ionic Liquids from Alkyloctamethylferrocenium Cations: Thermal Properties, Crystal Structures, and Magnetic Properties

Alkyloctamethylferrocenium salts with the Tf_2N anion ($[\text{Fe}(\text{C}_5\text{Me}_4\text{C}_n\text{H}_{2n+1})(\text{C}_5\text{Me}_4\text{H})][\text{Tf}_2\text{N}]$; Tf_2N = bis-(trifluoro-

methanesulfonyl)amide) were prepared, and their ionic liquid properties, thermal properties, crystal structures, and magnetic properties were investigated. The melting points of the Tf_2N salts were near room temperature, and decreased with increasing alkyl chain length up to $n = 8$ and then increased.

The salts with PF_6 and NO_3 anions were also prepared. The melting points of the PF_6 salts were higher than 100°C . Most of these salts exhibited phase transitions in the solid state. The sum of the entropies of the melting and solid phase transitions was nearly independent of the alkyl chain length for salts with short alkyl chains, whereas those for salts with longer alkyl chains ($n \geq 10$ for Tf_2N salts, $n \geq 6$ for PF_6 salts) increased with increasing alkyl chain length. Crystal structure determinations revealed that the short chain salts form simple alternately packed structures of cations and anions in the solid state, and that the long chain salts form lamellar structures, in which the alkyl chains are aligned parallel between the layers. The effects of magnetic fields on the crystallization of the paramagnetic ionic liquids were investigated, and revealed that the Tf_2N salts with $n = 4$ exhibited magnetic orientation when solidified under magnetic fields. The magnetic orientation was shown to be a bulk phenomenon, and the importance of the magnetic anisotropy of the crystal structure was suggested in comparison with the response of other Tf_2N salts.

4. Magnetic Resonance Investigation of Self-Doped Type TTFCOO and TTPCOO Family Salts

^1H -NMR and High-Field ESR measurements were carried out for self-doped type organic conductor, TTFCOO and TTPCOO derivatives. We found the conducting electrons both for TTFCOO and TTPCOO derivatives. But the spin susceptibility shows significant activation-type contribution and the ^1H -NMR spin-lattice relaxation rate, $^1\text{H}-T_1^{-1}$, shows a 1D electron spin-diffusion type relaxation for TTFCOO derivative. On the other hand, TTPCOO derivative shows metallic behavior down to the lowest temperatures. Detailed comparison between TTFCOO and TTPCOO salts is investigated.

References

- 1) S. Jin, X. Ding, X. Feng, M. Supur, K. Furukawa, S. Takahashi, M. Addicoat, M. E. El-Khouly, T. Nakamura, S. Irle, S. Fukuzumi, A. Nagai and D. Jiang, *Angew. Chem., Int. Ed.* **52**, 2017–2021 (2013).
- 2) T. Naito, T. Karasudani, K. Ohara, T. Takano, Y. Takahashi, T. Inabe, K. Furukawa and T. Nakamura, *Adv. Mater.* **24**, 6153–6157 (2012).
- 3) Y. Funasako, T. Inagaki, T. Mochida, T. Sakurai, H. Ohta, K. Furukawa and T. Nakamura, *Dalton Trans.* **42**, 8317–8327 (2013).

Award

FURUKAWA, Ko; SEST Young Investigator Award (2012).

* Present Address; Institute for Research Promotion Center for Instrumental Analysis, Niigata University

† carrying out graduate research on Cooperative Education Program of IMS with Yokohama National University

Organic Solar Cells

Department of Materials Molecular Science
Division of Molecular Functions



HIRAMOTO, Masahiro
Professor



KAJI, Toshihiko
Assistant Professor

NAKAO, Satoru
SHINMURA, Yusuke
KUBO, Masayuki

Post-Doctoral Fellow
Research Fellow
Research Fellow

YOKOYAMA, Kazuya
YOSHIOKA, Tadashi
KIKUCHI, Mitsuru
YAMASHINA, Yohei
ISHIYAMA, Norihiro
SUGIHARA, Hidemi

Research Fellow
Research Fellow
Research Fellow
Research Fellow
Graduate Student
Secretary

Organic solar cell (OSC) is recognized as a next generation solar cell. *pn*-control and nanostructure control of co-deposited films consisting two kinds of organic semiconductors are key issues for the development of OSC. Recently, we have established *pn*-control technique for single and co-deposited films of organic semiconductors.¹⁻³⁾ Moreover, we have developed a new method for producing phase-separated co-deposited films by introducing a co-evaporant molecules, which improves the carrier transport in the co-deposited film.⁴⁾

Here, we show the recent results on co-evaporant effect (Topic-1) and combination of doping and co-evaporant (Topic-2).

1. Nano-Structure Control of Organic Thin Films by Co-Evaporant Induced Crystallization

Nano-structure control of organic thin films is important for fabricating high performance organic electronic devices, such as organic transistors and OSCs. Especially, needle

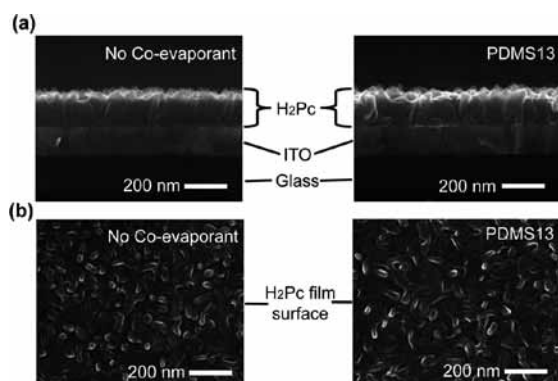


Figure 1. SEM images of 200-nm-thick H₂Pc film grown at 40 °C without co-evaporant/with PDMS. (a) Cross-sections. (b) Film surfaces.

growths of organic semiconductors sometimes roughen their film surface and the electronic devices composed of such films lose their robustness. Recently, we have proposed a new method of organic film growth, “co-evaporant induced crystallization,” and succeeded in crystallizing donor–acceptor blends, the key part of OSCs, based on small molecules by using a liquid as a non-sticking co-evaporant source during vacuum deposition of the blend film and showed striking enhancements of photocurrent. In this study, this new method is utilized for controlling the needle growth of metal-free phthalocyanine (H₂Pc) thin films. Nominally 200 nm of H₂Pc films were grown on indium tin oxide (ITO) coated glass substrates with substrate heating of 70 and 40 °C. The morphologies were observed by using scanning electron microscopy (SEM), and the crystallinities were confirmed by X-ray diffraction (XRD). Figure 1 shows SEM images of H₂Pc thin films grown at the substrate temperature of 40 °C with and without a co-evaporant, PDMS (polydimethylsiloxane). Similar lengths of H₂Pc needles are observed in the both films with/without co-evaporant. From grain size comparison, in contrast, the effect of the co-evaporant is clearly noticed as the grain size enlargement typically from 20 to 50 nm. This difference implies that the co-evaporant itself does not induce the needle growth, and that the needle growth is caused by the substrate heating, which is conventionally known effective for the crystallization of organic thin films. These results suggest that the co-evaporant enhances rather 2-dimensional-growth than 3-dimensional-growth of organic films.

2. *pn*-Homojunction Organic Solar Cells Formed in Phase-Separated Co-Deposited Films

Since the conductivity (σ) is the product of the mobility (μ) and the carrier concentration (n), *i.e.*, $\sigma = en\mu$, the resist-

ance (σ^{-1}) can be reduced by increasing both n , by means of doping, and μ , by means of co-evaporant introduction. Simultaneous control of the doping and phase-separation in co-deposited films was performed by using 4-sources co-evaporation consisting of H₂Pc, C₆₀, dopants, and co-evaporant (PDMS).

Figure 2 shows the energy diagram for the phase-separated H₂Pc:C₆₀ co-deposited films. For donor (Cs₂CO₃) doping, Fermi level (E_F) has shifted from the undoped value of 4.48 eV to 4.22 eV (green broken line, left) and is close to the C₆₀ conduction band (CB_{C60}). In contrast, for acceptor (V₂O₅) doping, E_F has shifted to 4.95 eV (green broken line, right) and is close to the H₂Pc valence band (VB_{H2Pc}). Clearly, the pn -control in the phase-separated co-deposited films were accomplished. Moreover, the shift in E_F is revealed to occur within the “bandgap of the co-deposited film.”

The doping was used to form pn -homojunctions in the phase-separated co-deposited films (Figure 3). In order to determine the precise extent of the photoactive layer beyond the depletion layer (Figure 4, blue shaded area), the J_{SC} for various p -type layer thickness (X) was calculated with the carrier generation efficiency following Gaussian profiles (Figure 3). Clearly, the curve with $\sigma = 250$ nm (green curve) agrees well with the observed short-circuit photocurrent (J_{SC}) (black dots), indicating that the photoactive layer extends 250 nm from the edge of the depletion layer.

This result means that the diffusion length of the minority carrier (electrons) reached extremely large value of 0.25 μ m. Thus, photogenerated electrons far from the pn -homojunction can reach the edge of the depletion region and be collected by the Ag electrode. Large minority carrier diffusion length is due to the large electron mobility ($\mu = 0.1$ cm²V⁻¹s⁻¹). On the other hand, a high hole concentration ($n = 1 \times 10^{17}$ cm⁻³) in the p -type C₆₀:H₂Pc film ensures hole extraction by the ITO electrode. This allows the fabrication of very thick cells up to 0.5 μ m thick with large values of fill factor (FF) of around 0.56.

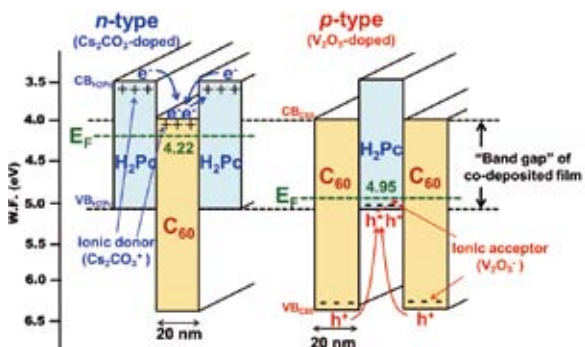


Figure 2. Phase-separated energy structure of C₆₀:H₂Pc co-deposited film doped with Cs₂CO₃-doped (n -type) and V₂O₅-doped (p -type) films.

Award

KAJI, Toshihiko; Young Scientist Research Paper Award from Molecular Electronics and Bioelectronics division of Japan Society of Applied Physics (2013).

The present cell is the first example of organic solar cell utilizing long minority carrier diffusion length like inorganic Si solar cells.

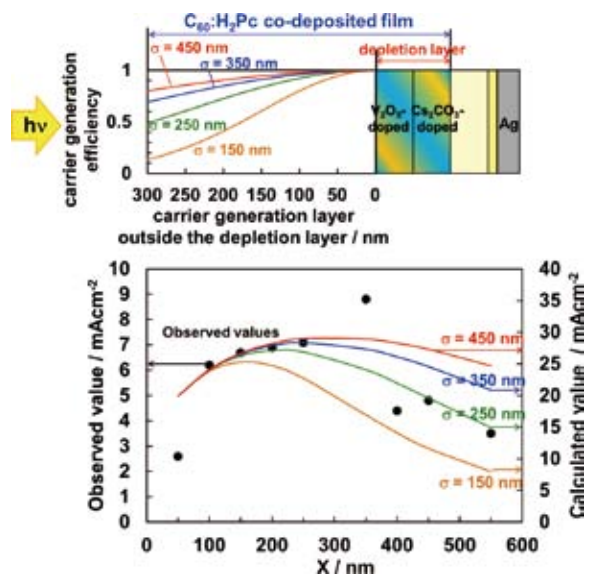


Figure 3. Dependence of calculated J_{SC} (solid lines) and observed J_{SC} (black dots) on p -layer thickness (X). Gaussian profiles of minority carriers outside the depletion layer are also shown.

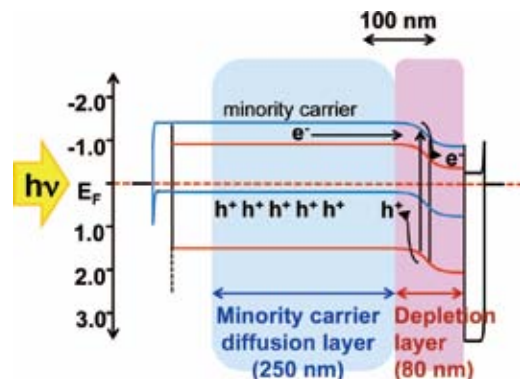


Figure 4. Energy structure of the cell. The depletion and minority carrier diffusion regions are indicated by the red and blue shaded areas, respectively.

References

- 1) M. Kubo, K. Iketaki, T. Kaji and M. Hiramoto, *Appl. Phys. Lett.* **98**, 073311 (2011).
- 2) Y. Shinmura, M. Kubo, N. Ishiyama, T. Kaji and M. Hiramoto, *AIP Adv.* **2**, 032145 (2012).
- 3) N. Ishiyama, M. Kubo, T. Kaji and M. Hiramoto, *Org. Electron.* **14**, 1793 (2013).
- 4) T. Kaji, M. Zhang, S. Nakao, K. Iketaki, K. Yokoyama, C. W. Tang and M. Hiramoto, *Adv. Mater.* **23**, 3320 (2011).

Two-Dimensional Polymers and Covalent Organic Frameworks

Department of Materials Molecular Science
Division of Molecular Functions



JIANG, Donglin
Associate Professor

GU, Cheng
DALAPATI, Sasanka
XU, Yan
NI, Huagang
JIN, Shangbin



NAGAI, Atsushi
Assistant Professor

IMS Fellow
IMS Fellow
Post-Doctoral Fellow
Visiting Scientist
Graduate Student

CHEN, Xiong
CHEN, Long
XU, Hong
WU, Yang
XU, Fei
HUANG, Ning
SUZUKI, Hiroko
HAMADA, MASAKO

Graduate Student
Graduate Student
Graduate Student
Graduate Student
Graduate Student
Secretary
Secretary

Two-dimensional polymers and their layered frameworks (covalent organic frameworks: COFs) are a class of crystalline porous materials that allow an atomically precise integration of components into a 2D or 3D periodicity. The recent synthetic progress has shown that 2D COFs are useful platform for designing conducting, where 2D polymer sheets are organized in a superimposed way to generate a layered architecture that provides periodic π pathways for charge-carrier transport.¹⁻⁷⁾

We pioneered the design and synthesis of COFs by integrating π -electronic units into the 2D polygon skeletons. In this year, we focus on our challenge for the molecular design of donor–acceptor COFs with periodically ordered electron donor–acceptor π -columnar structure and maximized bicontinuously segregated p-n interface, which provide a new molecular configuration and mechanism for optoelectronics and photovoltaics.

1. Charge Dynamics in 2D Polymers and COFs

The donor–acceptor heterojunction is a key structure in current technologies, including transistors, light-emitting diodes, and photovoltaics, because it controls the charge dynamics in the devices. Covalent organic frameworks (COFs) are crystalline molecular skeletons that allow atomically precise integration of building blocks into periodic array structures. In this regard, we have demonstrated arene, porphyrin, and phthalocyanine COFs that provide periodically ordered columnar arrays of π -components and show outstanding semiconducting and photoconductive properties. We

recently synthesized a donor–acceptor COF that gives rise to a periodically ordered bicontinuous heterojunction structure. This heterojunction structure provides ambipolar pathways for charge collection, and would be ideal for the current semiconducting devices that involve photoenergy transformations; however, the charge dynamics, which is a key mechanism that controls the energy transformation, remains unclear.

We determined the charge dynamics of a donor–acceptor COF using time-resolved spectroscopy. In the COF, the heterojunctions allow an ultrafast electron transfer from the donor to the acceptor columns. The light absorption is directly coupled with charge dissociation to generate free charges in the donor and acceptor π -columns within 2 ps. The stacked π -columns delocalize the charges, suppress charge recombination, and retain the charges for a prolonged period of time. The COFs enable rapid charge separation and exceptional long-term charge retention, thereby providing a key mechanistic basis to envisage the high potential of donor–acceptor COFs for photoelectric applications.

To clarify the charge dynamics in the solid-state COFs, we performed time-resolved electron-spin resonance (TR-ESR) spectroscopy. Before the 700-nm laser flash, the TR-ESR was silent over the entire magnetic field range. After the laser flash, the TR-ESR signal rapidly increased in intensity as a result of a very rapid charge separation. The TR-ESR signal exhibited an increase up to $t = 1.5 \mu\text{s}$ and then decayed slowly. Therefore, we monitored the TR-ESR spectra at $t = 1.5 \mu\text{s}$ as a function of the magnetic field and obtained a time-slice profile, which can be reproduced with a single emission-type Lorentzian with a g value of 2.0059 and a narrow spectral width of 0.75 mT. The g value of 2.0059 confirms the forma-

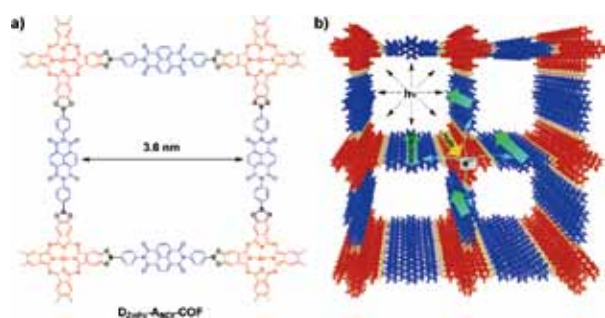


Figure 1. a) Structural representation of a donor–acceptor COF ($D_{ZnPc}-A_{NDI}$ -COF). Donor and acceptor units are shown in red and blue, respectively. The dotted black lines suggest the extension of periodic structures. b) Illustration of a 2×2 cell of the 0.8-Å slipped AA-stacking COF and photochemical events.

tion of $ZnPc^{*+}$ and NDI^{*-} species. The narrow spectral width of the COF is consistent with a weak magnetic dipolar interaction between two spins because they are spatially separated and delocalize in the donor and acceptor columns. The TR-ESR measurements at 80 K also confirmed the charge-separated state, as evidenced by a single emission-type Lorentzian profile with the same g value of 2.0059. Through curve-fitting of the time profiles to an exponential function given by $\Phi = \alpha \exp[-t/\tau_{CS}]$, where α , t , and τ_{CS} are the proportional factor, time, and lifetime, respectively, the τ_{CS} values of the solid-state COFs at 280 K was determined to be 1.8 μ s.

These dynamics provide mechanistic insights into the key photochemical processes involved in optoelectronics and photoenergy conversion systems and suggest that the donor–acceptor COFs are promising high-performance semi-conducting materials for use in applications.

2. Control Crystallinity and Porosity of Covalent Organic Frameworks through Managing Interlayer Interactions Based on Self-Complementary π -Electronic Force

COFs provide a useful skeleton for designing a new sort of organic semiconductors that feature columnar π -arrays periodically aligned at a nanometer-scale precision.^{3,6)} In this sense, the 2D COFs serve as a new platform for designing organic 2D materials with structural periodicity that is difficult to be achieved with other molecular architectures. However, controls over the crystallinity and porosity, which are key parameters in the applications, have been elusive.

We demonstrated the strategy using imine-linked porphyrin COFs, in which fluoro-substituted and non-substituted arenes at different molar ratios were integrated into the edge

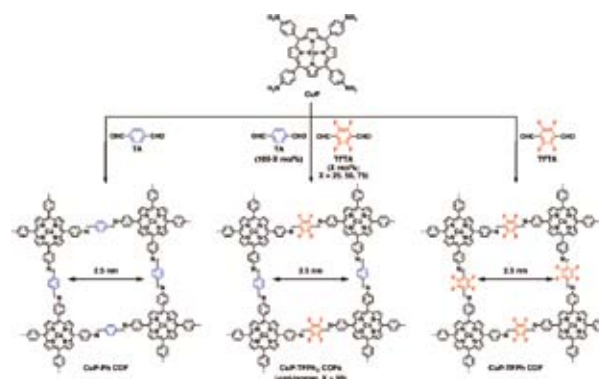


Figure 2. Schematic representation of the synthesis of COFs integrated with self-complementary π -electronic interactions (CuP-TFP $_X$ COFs, $X = 25, 50,$ and 75) and the CuP-Ph COF and CuP-TFP COF controls.

units (Figure 2). The porphyrins occupy the vertices and the arene units locate the edges of mesoporous two-dimensional COFs.

We demonstrated the control of COFs using self-complementary π -electronic interactions. Computational studies in conjunction with structural resolutions reveal that the self-complementary π -electronic force maximizes the total crystal stacking energy and minimizes the unit cell size. As a result, the COFs show an improved crystallinity and enhanced porosity, with the greatest effects observed when the interactions are strongest. Together with a prominent effect on changing the π -cloud distribution in the framework and lowering the HOMO-LUMO gap, the present work suggests a new means to designing COFs through managing the interlayer interactions.

References

- 1) Y. Xu, S. Jin, H. Xu, A. Nagai and D. Jiang, *Chem. Soc. Rev.* **42**, 8012–8031 (2013) (Cover Page).
- 2) X. Liu, Y. Xu, Z. Guo, A. Nagai and D. Jiang, *Chem. Commun.* **49**, 3233–3235 (2013).
- 3) A. Nagai, X. Chen, X. Feng, X. Ding, Z. Guo and D. Jiang, *Angew. Chem., Int. Ed.* **52**, 3770–3774 (2013) (Hot Paper).
- 4) S. Jin, X. Ding, X. Feng, M. Supur, K. Furukawa, S. Takahashi, M. Addicoat, M. E. El-Khouly, T. Nakamura, S. Irle, S. Fukuzumi, A. Nagai and D. Jiang, *Angew. Chem., Int. Ed.* **52**, 2017–2021 (2013) (Inside Cover).
- 5) X. Chen, M. Addicoat, S. Irle, A. Nagai and D. Jiang, *J. Am. Chem. Soc.* **135**, 546–549 (2013).
- 6) Y. Xu, A. Nagai and D. Jiang, *Chem. Commun.* **49**, 1591–1593 (2013) (Inside Cover).
- 7) X. Feng, Y. Dong and D. Jiang, *CrystEngComm.* **15**, 1508–1511 (2013).

Award

JIN, Shangbin; CSJ presentation Award.

Solid State NMR for Molecular Science

Department of Materials Molecular Science
Division of Molecular Functions



NISHIMURA, Katsuyuki
Associate Professor



IIJIMA, Takahiro
Assistant Professor



TANIO, Michikazu
IMS Research Assistant Professor

We are working on methodology and hardware developments of solid state NMR and structural biology and materials science. In the following, we show studies of peripheral membrane proteins and inorganic compounds based on NMR.

1. NMR Analysis of Intramolecular Allostery in the Phospholipase C- δ 1 Pleckstrin Homology Domain

Proteins are generally activated by interactions with ligands, such as proteins, lipids, peptides, nucleotides, ions, photons, odorants, or other chemical compounds. Ligand binding usually induces changes in the protein conformation and dynamics, which also occur at distal sites away from the ligand-binding site in the protein molecule through intramolecular signal transductions, causing allosteric regulation of protein functions. Although elucidation of allosteric mechanisms is expected to be useful for regulations of protein functions and for allosteric drug designs, the detailed molecular mechanisms remain unclear.

Our previous study suggested the existence of intramolecular allosteric interactions in the phospholipase C (PLC)- δ 1 pleckstrin homology (PH) domain.¹⁾ The PLC- δ 1 PH domain binds to phosphatidylinositol 4,5-bisphosphate (PIP₂) in the cell membrane, and inositol 1,4,5-triphosphate (IP₃), a product of PIP₂ hydrolysis by PLC- δ 1. Mutational analyses of the PLC- δ 1 PH domain demonstrated that conformational disruption of the characteristic short α -helix (α 2) from residues 82 to 87 results in reduced affinity for IP₃ and in thermal instability, and that the phenyl ring of Phe-87 contributes to effective stabilization of the IP₃-binding state.¹⁾ However, the α 2-helix does not make direct contact with IP₃ in the crystal structure of the PLC- δ 1 PH domain complexed with IP₃, and our findings therefore indicate that the α 2-helix indirectly interacts with the IP₃-binding site through intra-

molecular allosteric interactions. In this study, we investigated the detailed molecular mechanisms of intramolecular allosteric interactions among spatially separated sites in the PLC- δ 1 PH domain by using NMR.²⁾

To detect the local environmental changes in the protein induced by ligand binding and site-specific mutations, we analyzed the ¹H-¹⁵N HSQC NMR spectra of selectively [α -¹⁵N]Lys-labeled PLC- δ 1 PH domain and its mutants in the presence and absence of IP₃. In the wild-type protein, IP₃-dependent chemical shift changes were observed for all lysine signals, indicating that IP₃ binding affects the local environments at all lysine residues. Chemical shift perturbation (CSP) analyses for the wild-type protein demonstrated that more

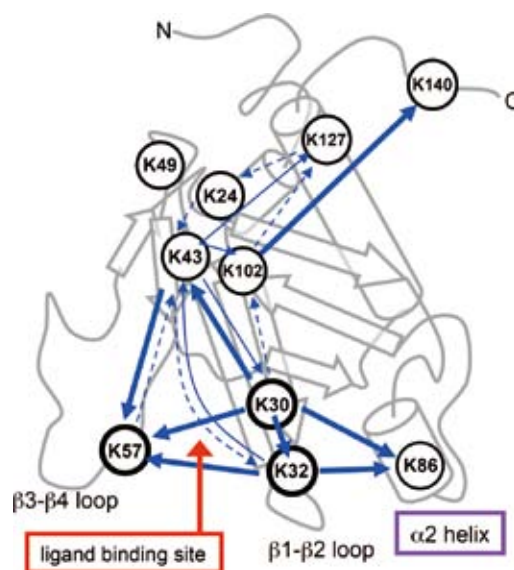


Figure 1. Graphical summary of the mutational effects on the PLC- δ 1 PH domain. The bold, thin and dashed blue arrows indicate directions from mutated residues to affected residues with major, medium and minor CSP changes, respectively.

marked changes of chemical shifts were observed for Lys-43, Lys-102, and Lys-127, of which the α -nitrogen atoms are located far from the IP₃-binding site consisting of Lys-30, Lys-32, and Lys-57, suggesting that more drastic changes occurs at these distal sites on IP₃ binding.

If specific IP₃ binding induces local environmental changes at distal sites, mutations at the ligand-binding site would also affect local environments at spatially separated sites in the PLC- δ 1 PH domain. The mutational analyses for signal assignments demonstrated that the single lysine mutants, K30A, K32A, K43A and K102A, showed significant chemical shift changes of at least two signals with drastic CSP changes as compared with the lysine chemical shifts of the wild-type protein under the ligand-free state. The effects of single lysine mutations on the other lysine residues are graphically summarized in Figure 1. These results indicate that an interaction network mainly consisting of the side chains of Lys-30, Lys-32, and Lys-43, but not Lys-57 or Lys-86, exists in the ligand-free protein.

The IP₃ titration experiment of the wild-type protein also demonstrated that in the ligand-free state, the α 2-helix undergoes intermediate chemical exchange between at least two conformations with different population, and that IP₃ binding stabilizes one of the two conformations.²⁾ Interestingly, such stabilization of the α 2-helix (Lys-86) induced by IP₃ binding was also observed in F87Y, but not in K57A or F87A (Figure 2), indicating that the side chains of Lys-57 and Phe-87 contribute to stabilization of the IP₃-binding state, although Lys-57 does not contribute to the interaction network in the ligand-free state. Our results therefore strongly suggested that the pre-existing interaction network, mainly consisting of Lys-30, Lys-32 and Lys-43, in the ligand-free state is modified by IP₃ binding, resulting in formation of a new interaction network, in which Lys-57 and Phe-87 contribute to stabilization of IP₃-binding state.²⁾

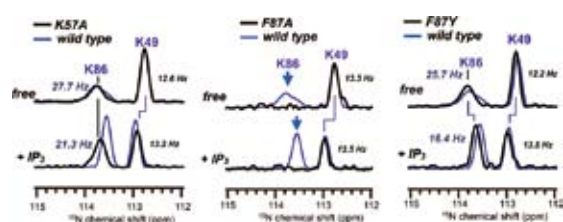


Figure 2. ¹⁵N projections around the Lys-86 signal of the ¹H-¹⁵N HSQC NMR spectra of [α -¹⁵N]labeled K57A (left), F87A (middle) and F87Y (right) in the absence (top) and presence of IP₃ (bottom) as compared with those of the wild-type protein (blue).

2. A DFT Study of Electron Absorption of Polyoxomolybdates with d¹ Electrons

Among molybdenum with an integer valence from Mo⁰ to Mo^{VI}, many Mo^V species are included in polyoxomolybdates of ϵ -Keggin anions and nano-sized oxides with characteristic shape. Localization of d¹ electrons of the Mo^V species has attracted much attention in terms of molecular design and solid state physics. Recently, we have found from solid-state

⁹⁵Mo NMR and DFT calculation that for {Mo₁₂(La)} ([PMo₁₂O₃₆(OH)₄{La(H₂O)_{2.75}Cl_{1.25}}₄·27H₂O) having eight d¹ electrons in a molecule, (i) there are two different molybdenum sites with population of 2:1 and (ii) they are basically corresponding to the species of Mo^V and Mo^{VI}, but some of the d¹ electrons are delocalized. This is a somewhat surprising result, because no intervalence charge-transfer bands for Mo^V to Mo^{VI} have been observed so far. In this work, we calculated electron absorption spectra of some polyoxomolybdates including {Mo₁₂(La)} by DFT.

DFT calculation of the absorption spectra was implemented by the ADF2013.01 software. The local density approximation of VWM augmented with the Becke-Perdew GGA was employed for the exchange-correlation functional. The TZ2P or DZ all-electron basis set was used. Only allowed transitions were used for calculation of the absorption spectra.

Figure 3 shows the electron absorption spectra of polyoxomolybdates in the range of wavelength 400–1,400 nm obtained by DFT. Figure 3(i) is the spectrum of {Mo₁₆} ([Me₃NH]₆[H₂Mo^V₁₂O₂₈(OH)₁₂(Mo^{VI}O₃)₄·2H₂O), where twelve d¹ electrons are localized to form six Mo^V–Mo^V bonds of the ϵ -Keggin core. The relatively strong peak is only at around 430 nm that explains the brown color of this crystal. The weak peaks at ca. 590 and 655 nm are due to the d–d transition of the d¹ electrons of Mo^V. Figure 3(ii) shows the electron absorption spectrum of {Mo₁₂(La)}. It is found that the number of the peak increased both in the visible-light and near-infrared regions for {Mo₁₂(La)}. However, the absorption with short-wavelength visible light is consistent with the bark color of the crystal. Also, the intensity of the increased d–d transitions with wavelength of the near-infrared region would be not enough for the electron transition to be observed. Therefore, the slight delocalization of the d¹ electrons of {Mo₁₂(La)} seems to be plausible.

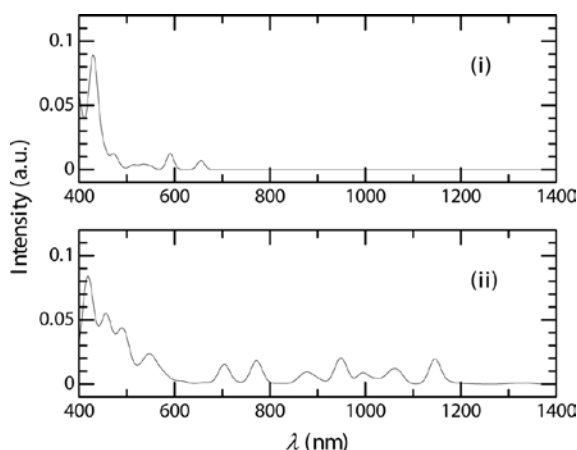


Figure 3. Electron absorption spectra for the polyoxomolybdates of (i) {Mo₁₆} and (ii) {Mo₁₂(La)} obtained by DFT calculation.

References

- 1) M. Tanio and K. Nishimura, *Anal. Biochem.* **431**, 106–114 (2012).
- 2) M. Tanio and K. Nishimura, *Biochim. Biophys. Acta* **1834**, 1034–1043 (2013).

Development of Novel Heterocyclic Compounds and Their Molecular Assemblies for Advanced Materials

Safety Office



TOMURA, Masaaki
Assistant Professor

Heterocycles containing sulfur and/or nitrogen atoms are useful as components of functional organic materials since heteroatoms in their rings are helpful to stabilize ions or ion-radical species. In addition, intermolecular interactions caused by heteroatom contacts can be expected to form unique molecular assemblies. In this project, novel functional organic materials based on various heterocycles were synthesized and their physical and structural properties were investigated.

1. Molecular and Crystal Structure of Cyananilic Acid Dihydrate

Cyananilic acid shows both electron accepting and proton

donating properties. Supramolecular synthons formed with cyananilic acid have been used for constructing a variety of molecular networks. A molecular and crystal structure of cyananilic acid was reported as its hexahydrate derivative in 1975.¹⁾ We have found a novel hydrate isomer of cyananilic acid, dihydrate derivative. Cyananilic acid dihydrate crystallizes in the triclinic $P\bar{1}$ space group with one molecule in the unit cell. Cell parameters are $a = 4.940(6)$ Å, $b = 7.064(8)$ Å, $c = 7.404(8)$ Å, $\alpha = 109.20(2)^\circ$, $\beta = 94.73(1)^\circ$, $\gamma = 102.27(1)^\circ$ and $V = 235.2(5)$ Å³. The cyananilate dianion molecule is planar with an r.m.s. deviation of 0.011(2) Å and is located on an inversion center. The cyananilate molecules are linked via the oxonium ions with intermolecular O–H...O and O–H...N interactions.

Reference

1) E. K. Anderson and I. G. K. Anderson, *Acta Crystallogr., Sect. B* **31**, 379–383 (1975).

Multifunction Integrated Macromolecules for Molecular-Scale Electronics

Safety Office



TANAKA, Shoji
Assistant Professor

Recently a single electron tunnel device (SET) has attracted much attention. In this project, to establish an innovative fabrication process for SET systems, we have been developing stepwise synthetic protocols for mono-molecular single-electron tunnel devices (MOSET) and their integrated circuits.

different reactivity for metal-catalyzed coupling reactions. Thus, a selective and stepwise cross coupling will lead to more complicated macromolecular systems. Now we have been developing the synthetic protocols for mono-molecular integrated circuits such as single electron memory and counter, using these building blocks **1-16** (Figure 1(b)).

1. Upgrade of Building Blocks toward Higher Integration of Single-Electron Tunnel Devices

We have developed a generally applicable stepwise synthetic protocol for basic mono-molecular single-electron tunnel devices starting with our versatile building blocks (**1-4**) (Figure 1(a-b)). In order to advance to the next stage of nanofabrication, we have prepared a new set of molecular building blocks (**5-16**) in view of recent progress in cross coupling reactions of C–Cl and C–H bonds of heterocycles. The end points of these molecular blocks have significantly

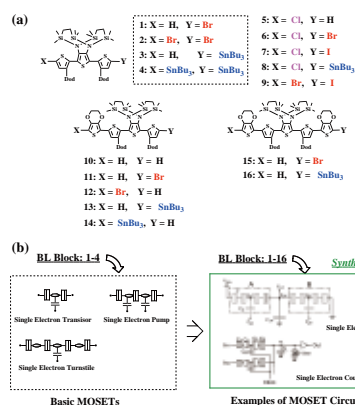


Figure 1. (a) Molecular structure of building blocks. (b) A strategy for mono-molecular MOSETs integration.

Visiting Professors



Visiting Professor

ASAKURA, Tetsuo (*from Tokyo University of Agriculture and Technology*)

Determination of Molecular Structure with Ultra Fast MAS under High-Field NMR

In single crystal X-ray diffraction analyses of peptides and proteins, it is well-known that the co-ordinates of carbon, nitrogen and oxygen atoms can be obtained in high accuracy, but enough accuracy cannot be obtained for those of hydrogen. Therefore we are trying to determine the accurate ^1H positions by the combination of NMR observation by ultra fast magic angle spinning under high field magnetic field and accurate ^1H NMR chemical shift calculation. We are applying this novel analytical technique to determine the structures of silk fibroins before and after spinning together with their model peptides. Since such a ^1H information is sensitive to both the intra- and inter-molecular structures, it is especially useful in molecular design of biomaterials with silks.



Visiting Professor

TAKENOBU, Taishi (*from Waseda University*)

Electronic Phase Control of Molecular Materials by Electric Double Layer Transistors

Charge carrier control is one of the key issues in the development of solid state physics and novel functional devices. Beyond the simple enhancement of conductivity, high charge carrier accumulation can realize various phenomena, such as phase transition, magnetic ordering, and superconductivity. Electric double layers, formed at solid/electrolyte interfaces, induce extremely large electric fields, huge specific capacitance and high charge carrier accumulation, and, as the results, this method opens new route for novel functionalities. Because molecular materials have large variety of electronic and magnetic properties, we are trying the combination of molecular solid and electric double layer transistors to discover novel phase transitions and functional devices.



Visiting Associate Professor

KANEMOTO, Katsuichi (*from Osaka City University*)

Optical and ESR Characterizations of Organic Semiconductor Devices

π -conjugated molecules and polymers have been the subject of much interest due to their potential device applications such as LEDs, solar cells, and field-effect transistors. Their remarkable electronic properties are owing to excitons and carriers created by photoexcitation or bias impression. The main purpose of our research is to characterize the determinant roles of the excitons and carriers on the device operation, through *in situ* optical and ESR measurements for operating organic devices. Recently, we found that a transient current is induced at the moment of ESR in polymer diodes under photoirradiation. The transient current was compatible with a steady-state photocurrent and found to arise from a change of polarization induced by ESR.